communications materials

A Nature Portfolio journal

Article

https://doi.org/10.1038/s43246-025-00790-7

Bilayer sol-gel system for local prevention in prosthetic joint infections and osteointegration improvement

Antonia Jiménez-Morales[1,2,3], **Ángela Solís-Garrido**[1] ✉, **Beatriz Toirac**[1], **Aranzazu Mediero**[4], **Bruna Costa**[5], **Francisca Mulero**[6], **Óscar Murillo**[7], **Miguel Monclús**[8], **Jaime Esteban**[2,9] & **John Jairo Aguilera-Correa**[2,9] ✉

Prosthetic joint infection (PJI) is one of the most severe complications associated with arthroplasties. Here we evaluate a bilayer coating system designed for both PJI prevention and osteoinduction. The outer layer is loaded with levofloxacin and linezolid, providing broad-spectrum antibiotic effects in the short term, while the inner layer, loaded with dipyridamole, promotes osteointegration. We then deposit the coatings onto powder-metallurgical titanium substrates. The antibacterial outer layer effectively inhibits biofilm formation and planktonic bacterial growth, targeting both Gram-positive and Gram-negative bacteria. The osteostimulating inner layer, containing the highest dipyridamole concentration, enhances in vitro mineralisation. In vivo the bilayer system significantly reduces infection symptoms and bacterial load in the femur of *S. aureus*-infected mice with coated implants. Additionally, it promotes bone metabolism at the implant-bone interface, resulting in increased bone mineral content and density.

One of the most concerning complications in arthroplasty is the development of an infection, which can have severe consequences for the patient. Prophylaxis is typically performed through the administration of broad-spectrum antibiotics, either orally or parenterally. Nevertheless, this strategy may be ineffective due to factors such as inadequate vascular perfusion at the infection site. As a result, local therapies have been proposed as a suitable alternative to directly target the implant-periprosthetic tissue interface.

Even though the incidence of prosthetic joint infections (PJI) may appear quite low (hip: 0.2–1.5%; knee: 0.4–1.5%; shoulder: 0.8–2.0%[1,2]), it is progressively increasing. PJI is associated with high morbidity, surgical complications, and significant economic costs[3]. In 2020, the total number of prosthetic replacements reached 4 million, corresponding to a financial burden of approximately $16 billion[4]. The impact of prosthetic joint infections (PJIs) is further highlighted by their mortality rate, which is around 20% of infected patients[5]. Furthermore, the 5-year mortality rate for PJIs surpasses that of other conditions such as breast cancer, melanoma, and Hodgkin's lymphoma[6].

Gram-positive cocci, mainly *Staphylococcus aureus* and coagulase-negative staphylococci, are the most common pathogens responsible for PJI, accounting for up to 77% of cases[2,7,8]. However, Gram-negative bacilli, including fermenting and non-fermenting species such as *Escherichia coli* and *Pseudomonas aeruginosa*, are becoming increasingly relevant as causative agents of PJI[7].

Following prosthesis implantation surgery, necrotic and/or avascular tissue may persist at the prosthesis-tissue interface[9], leading to inadequate systemic antibiotic prophylaxis. In light of this, local prophylaxis becomes highly advisable. Although a plethora of different locally preventive strategies have been developed, we have previously demonstrated that sol-gel coatings serve as effective carriers for different antibiotics[10]. Specifically, when loaded with moxifloxacin, these coatings have been shown to

---

[1]Materials Science and Engineering and Chemical Engineering Department, Carlos III University of Madrid, Av. de la Universidad, 30, 28911 Leganés, Madrid, Spain. [2]CIBERINFEC-CIBER de Enfermedades Infecciosas, Av. Monforte de Lemos 5, 28029 Madrid, Spain. [3]Álvaro Alonso Barba Technological Institute of Chemistry and Materials, Carlos III University of Madrid, Av de la Universidad 30, 28911 Leganés, Madrid, Spain. [4]Bone and Joint Unit, IIS-Fundación Jiménez Díaz, UAM, Av. de los Reyes Católicos, 2, Moncloa - Aravaca, 28040 Madrid, Spain. [5]BioEngineered Surfaces, i3S, Instituto de Investigação e Inovação em Saúde, Universidade do Porto, Rua Alfredo Allen, 208, 4200-135 Porto, Portugal. [6]Molecular Imaging Unit, Spanish National Cancer Research Centre (CNIO), C. de Melchor Fernández Almagro, 3, Fuencarral-El Pardo, 28029 Madrid, Spain. [7]Infectious Diseases Department and Laboratory of Experimental Infection, Hospital Universitari de Bellvitge, IDIBELL, Universitat de Barcelona, Carrer de la Feixa Llarga, s/n, 08907 L'Hospitalet de Llobregat, Barcelona, Spain. [8]IMDEA Materials Institute, C. Eric Kandel 2, 28906 Getafe, Madrid, Spain. [9]Clinical Microbiology Department, IIS-Fundación Jiménez Díaz, UAM, Av. de los Reyes Católicos, 2, Moncloa - Aravaca, 28040 Madrid, Spain. ✉e-mail: ansolisg@ing.uc3m.es; john.aguilera@fjd.es

completely prevent in vivo PJI development caused by *S. aureus* and *E. coli*. Since PJIs can be caused by both a Gram-positive and Gram-negative bacteria, an ideal local prophylactic strategy should be capable of preventing infections from both types simultaneously. This can be achieved by incorporating at least two antibiotics, each targeting a specific bacterial group[11].

In addition to infection prevention, promoting bone tissue growth is a valuable property in prosthetic materials[12]. Our previous studies demonstrated that incorporating phosphite into sol–gel coatings enhances osteoblastic growth[13]. Furthermore, sol–gel technology allows for precise control over degradation through exhaustive synthesis studies, where factors such as temperature, humidity, agitation, and the use of a closed dry box are tightly regulated[10,13–16]. These hybrid organo-inorganic coatings can also be loaded with osteointegrative molecules such as dipyridamole.

Dipyridamole was selected for our coating due to its ability to promote bone formation in the periprosthetic tissue. It exerts its effects by indirectly activating adenosine receptors, which are involved in bone remodelling[17,18]. Adenosine is generated by hydrolysis of adenine nucleotides, both intracellularly and extracellularly, and acts locally to mediate its pharmacological and physiological actions via activation of selective G protein-coupled receptors (A1, A2A, A2B, and A3)[19]. Previous studies have demonstrated that A2A receptor stimulation inhibits osteoclast differentiation and function[20,21], while A2A deletion leads to osteopenia in mice[21]. Moreover, activation of the A2A receptor has been shown to reduce bone porosity and erosion in a murine model of osteolysis, resulting in an increase in bone volume compared to control bones[21]. Additionally, it was found that direct and indirect activation of the A2A receptor stimulates new bone formation as well as rhBMP-2 (bone morphogenetic protein 2)[18]. Other studies demonstrated that coating scaffolds printed with HA/β-TCP using dipyridamole enhanced bone regeneration in critical bone defects[22]. Furthermore, it has been confirmed that dipyridamole reversed the bone-deleterious effect of tenofovir, an antiretroviral drug that blocks ATP transport, both in vitro and in vivo[23].

The aim of this study was to evaluate a bilayer system composed of two different coatings designed for both PJI prevention and osteoinduction. The outer layer, loaded with levofloxacin (effective against both Gram-negative and Gram-positive bacteria) and linezolid (primarily active against Gram-positive bacteria), was designed to provide a broad-spectrum antibiotic effect within the first 48 h after surgery. This layer was tested for its efficacy in in vitro biofilm development and treatment, cytotoxicity, and cell proliferation. The inner layer, loaded with dipyridamole and designed for long-lasting degradation (over 35 days post-surgery), was evaluated in cell viability, cell proliferation, and bone mineralisation studies. Finally, the combined effect of the bilayer system was assessed in an in vivo murine model.

Results and discussion

Synthesis characterisation of sols and xerogels: outer and inner layer

FT-IR sol–gel spectra, after 24 h of synthesis, are shown in Fig. 1A, B, and the solid-state ^{29}Si-NMR spectra of the xerogels of the obtained xerogels are shown in Fig. 1C, D.

The formation of the siloxane network was studied by identifying bands associated with the vibrational modes of the Si–O–Si chains, detected at ~815 cm^{-1} (weak band), ~1060 cm^{-1} and ~1160 cm^{-1}. The Si–O–Si chain results from the condensation process. A broad band was also observed at ~3420 cm^{-1}, which is related to the vibrational modes of the –OH groups, including the Si–OH bonds, which are products of sol–gel hydrolysis[24–26]. Residual products from the synthesis were also detected, with bands observed between 3200 and 3500 cm^{-1}, attributed to vibrations of –OH groups that may be due to traces of water and alcohol or terminal Si–OH groups. A band around ~890 cm^{-1} was associated with the vibration of the terminal Si–OH[24–27].

Regarding the outer layer, the presence of phosphorus and its incorporation into the siloxane network was confirmed by the appearance of bands at 1254 and ~850 cm^{-1}, corresponding to the stretching vibration of the P = O bond[13] and bending of the Si–O–P bond, respectively[28]. Absorption bands around 2960 and 2900 cm^{-1} were related to C–H bonds[27,29,30]. Bands at ~1720 cm^{-1} and ~1640 cm^{-1} were associated with the stretching vibrations of carbonyl (C = O) and C = C groups, respectively, as well as the methacrylate groups from the MAPTMS precursor[15]. A band at ~1450 cm^{-1} was identified as the deformation modes of symmetric and asymmetric CH_3 groups[30]. The asymmetric and symmetric stretching vibrations of C–O and C–O–C bonds were identified around ~1320 and 1300 cm^{-1}. Finally, a band at ~950 cm^{-1} was attributed to the C = C vibration from the C = C–C = O group[15].

In contrast, the inner layer showed bands related to the organic components from the MTMOS precursor, with vibrations associated with short methyl chains at 1275 cm^{-1} and the vibration associated with Si–C bond at 1450 cm^{-1} [31]. Additionally, C–H bonds were identified in bands around 2870 and 2950 cm^{-1} [24–26]. No differences were observed in the shapes of the absorption bands compared to control formulations, nor the appearance of new bands in the spectra. This suggests that the insertion of linezolid, levofloxacin (either together or separately), and dipyridamole in the different control sol–gel syntheses does not affect the formation of the characteristic reactions involved in this process. Furthermore, it indicates that the siloxane network remains unmodified. However, considering the very low concentration of the drugs, any related bands may be too weak to be detected in this study.

The degree of network cross-linking was studied by ^{29}Si-NMR for non-loaded xerogels, LEV-LNZ xerogels, and the samples with the maximum load of drugs (Fig. 1C, D). In ^{29}Si-NMR spectroscopy, T^n-type structures represent silicon atoms that are bonded to an organic chain, with three possible oxygen-bridging bonds remaining with other silicon atoms. The superscript n indicates the number of siloxane bonds, which can range from 0 to 3. Q^n-type structures represent Si atoms with four hydrolysable alkoxy groups, and their superscript n can range from 0 to 4. In the case of the formulations presented in this study, the T species are related to the MAPTMS in the outer layer and MTMOS in the inner layer. Q species, on the other hand, are identified with the TMOS and TEOS precursors for the outer and inner layers, respectively[15,29].

T^2, T^3, Q^3, and Q^4 signals were observed in all xerogels at −57, −66, −101, and −110 ppm, respectively. A high degree of crosslinking in the siloxane network was observed in all systems, with the absence of non-hydrolysed species or those with a single siloxane bond in both precursors. The T^3 signal was predominant over the T^2 in the MAPTMS/MTMOS precursors. In the antibiotic formulations, the same behaviour was observed with Q^3 over Q^4 in the TMOS bands. In the outer coating, a signal at ~12.5 ppm it was also identified as P=O, corresponding to the formation of P=O bonds in the sol–gel network surrounding Si atoms. The integration mechanism of this compound has been previously described by García-Casas et al.[13].

To summarise, the outer coating xerogels demonstrated the formation of three-dimensional networks, primarily dominated by fully condensed siloxane MAPTMS (T^3). This was followed by fully condensed TMOS silane (Q^3 and Q^4), accompanied by P = O and T^2. In the inner coating, the highest signal intensity was observed in T^3. These results indicate that the formulations exhibited a high degree of cross-linking, as the detected species are either fully condensed (T^3 and Q^4) or nearly fully condensed (T^2 and Q^3). Furthermore, it can be concluded that the network predominantly composed of MTMOS silane, as expected based on the molar ratio of the silanes. In both layers, no significant differences were observed between spectra, suggesting that the introduction of the drugs did not alter the cross-linking of the sol–gel network.

Physicochemical characterisation of the coatings: morphological characterisation (SEM)

Supplementary Fig. 1 presents coating micrographs captured using a backscattered electron detector. The images reveal uniform, homogeneous, crack-free, and poreless layers.

For the adhesion test, ASTM D 3359-02[32] was adapted to the available equipment. All coatings achieved a 4B rating, indicating that less than 5% of

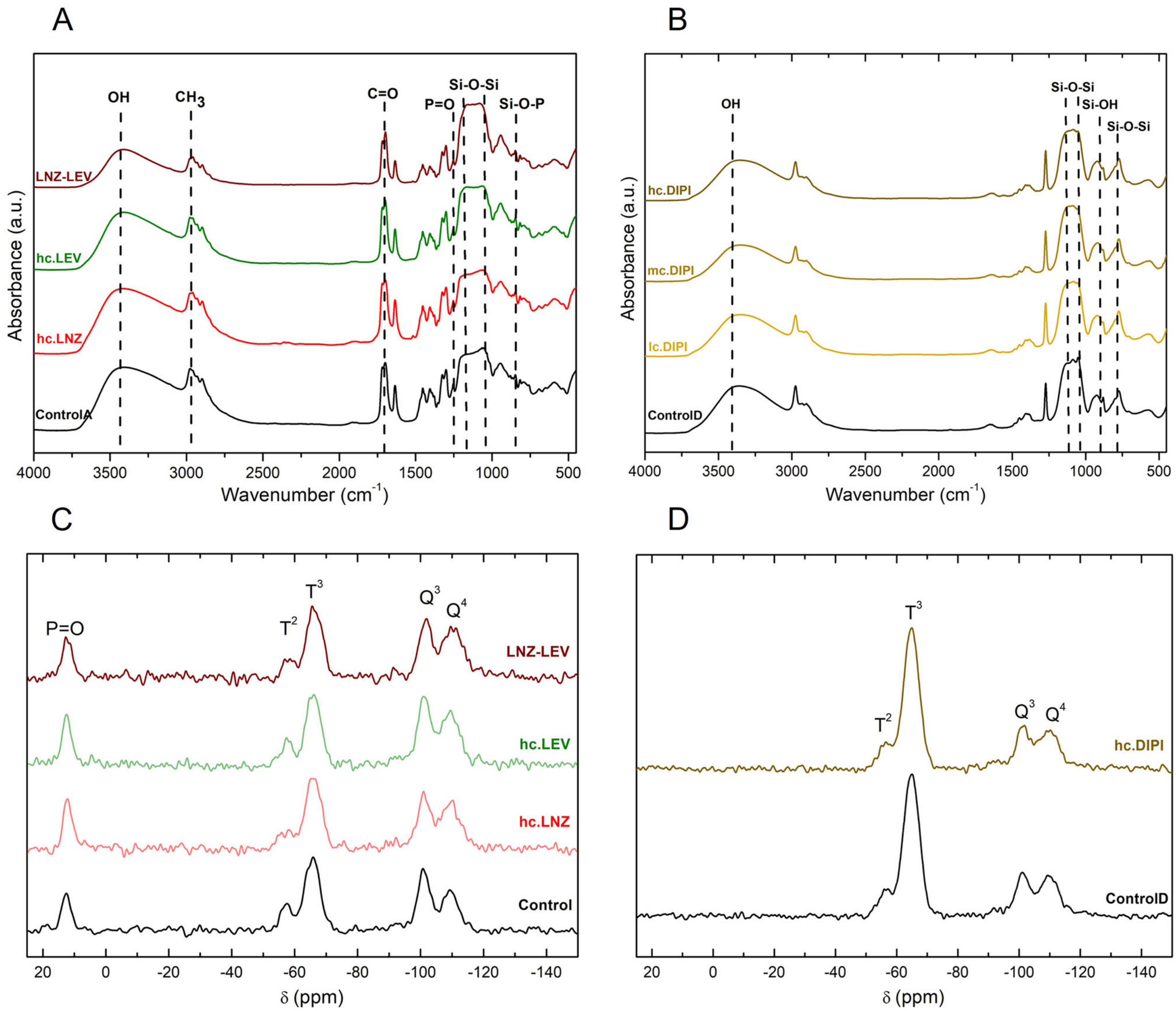

Fig. 1 | Structural characterisation of control and treated coatings. Representative FT-IR absorption spectra (**A**) and ^{29}Si-NMR spectra (**C**) of ControlA, hc.LNZ, hc.LEV, and LNZ-LEV. FT-IR absorption spectra (**B**) and ^{29}Si-NMR spectra (**D**) of ControlD, lc.DIPI, mc.DIPI, and hc.DIPI (outer and inner layers, respectively).

the coating was removed by the adhesion tape, except for hc.LNZ (Supplementary Fig. 2B). The slightly lower adhesion observed in hc.LNZ, suggest that this coating exhibited a more gelled sol-gel network, with fewer hydrolysed silanes bonding to the substrate surface. This result aligns with the ^{29}Si-NMR findings, were hc.LNZ showed the highest proportion of fully condensed TMOS silanes alongside a significant presence of fully condensed MAPTMS silanes. Achieving strong adhesion is crucial for the successful application of these coatings in prosthetic joint surgeries.

Physicochemical characterisation of the coatings: morphological characterisation (SEM)

The surface topography of the coatings was analysed using atomic force microscopy in non-contact mode (Supplementary Fig. 2). The 3D representations (Supplementary Fig. 2, left) and 2D images (Supplementary Fig. 2, middle) correspond to $5 \times 5\ \mu m^2$ topographic scans, while the right-hand images depited the bidimensional surface profiles. The coatings studied included ControlA, ControlD, maximum concentration LEV and LNZ samples, their combination (LNZ-LEV), hc.DIPI and the bilayer coating.

AFM imaging of the outer layer revealed highly smooth surfaces with nanometric protrusions or pores. However, the hc.LNZ samples displayed numerous larger protuberances (5–30 nm), attributed to the incorporation of the organophosphorus compound, exceeding those observed in ControlA. The LNZ-LEV coating exhibited a smooth surface with isolated nanopores.

In contrast, AFM scans of the inner layer images showed microscale roughness, characterised by micropores and variable height variations. The bilayer coating demonstrated a granular texture with random growth patterns.

Roughness analysis, conducted using $40 \times 40\ \mu m^2$ AFM scans, is summarised in Table 1. The LNZ-LEV coating exhibited lower slope roughness parameters (S_a, S_q, and S_z) than hc.LEV and hc.LNZ, indicating a smoother surface. These parameters also confirmed that the coatings enhanced the smoothness of the metallic substrate. No statistically significant differences were found in the roughness parameters of the inner

Table 1 | Antibiotic concentration in outer/antibiotic layer

Identification	Levofloxacin concentration (mg/mL)	Linezolid concentration (mg/mL)
ControlA	0.00	0.00
hc.LEV	1.84	–
hc.LNZ	–	2.46
LNZ-LEV	1.84	2.46

Table 2 | Surface roughness parameters and their standard deviations obtained by AFM image analysis

Surface	S_a (nm)	S_q (nm)	S_z (µm)
TiPM	169.79 ± 42.80	227.96 ± 45.05	2.111 ± 0.564
ControlA	9.61 ± 2.43	12.43 ± 3.03	0.087 ± 0.025
hc.LNZ	38.95 ± 13.84	67.85 ± 55.44	0.870 ± 0.748
hc.LEV	16.60 ± 13.74	19.60 ± 15.14	0.079 ± 0.036
LNZ-LEV	7.73 ± 2.66	9.81 ± 3.47	0.068 ± 0.023
ControlD	31.60 ± 7.74	40.68 ± 10.65	0.297 ± 0.056
hc.DIPI	68.51 ± 42.29	83.94 ± 48.19	0.474 ± 0.146
Bilayer	13.10 ± 3.10	18.30 ± 3.20	0.223 ± 0.066

S_a average roughness, S_q root average square roughness, S_z maximum height. Results are the average of 8 measurements from 40 × 40 µm^2 scans.

coatings, except for the maximum pore height (S_z). In the bilayer system, the slope roughness values were low, indicating a relatively flat or low-roughness surface[31,32].

The roughness parameters confirmed that the coatings produced exceptionally smooth surfaces compared to uncoated TiPM, consistent with SEM observations that showed uniform, crack-free coatings with no uncoated areas.

To further characterise the surface, coating thickness and hydrophobicity (contact angle) were evaluated (Table 2). The outer layer thickness was approximately 12 µm, with no statistically significant differences between samples. Contact angle measurements also showed no meaningful variation.

For the inner layer, the average thickness was around 9.5 µm, with a contact angle of 87°. In contrast, the bilayer system exhibited a greater thickness of 13 µm, like that of the antibiotic-loaded coatings, with no significant statistical differences between them.

These results demonstrate that the coatings effectively modified the surface characteristics without significant differences in thickness or hydrophobicity between the different formulations.

Coating degradation study

The degradation of the coatings was evaluated using electrochemical impedance spectroscopy (EIS).

Figure 2 presents Bode diagrams for antibiotic coatings at 4, 12, and 24 h (Fig. 2A, B) and osteoinductive/bilayer coatings after 35 days (Fig. 2C, D). SEM micrographs of the samples after 24 h and 35 days of immersion are shown in Figs. S3A–S3E. All tests were conducted in PBS at 37 °C.

Outer layer. The systems demonstrated stability over 24 h, as evidenced by the absence of significant variations in the impedance modulus at 10^{-2} Hz (≈2×10^5 Ω cm^2 across all samples). The phase angle values at medium-to-high frequencies followed a similar trend in all systems, increasing over time. This suggests an expansion of the active area due to progressive moistening of the coatings, leading to greater electrolyte exposure[33,34].

Over time, impedance modulus values at medium-high frequencies increased, potentially due to pore blocking by insoluble salts from the electrolyte, coating swelling, and/or the formation of a passive titanium oxide layer.

SEM micrographs (Supplementary Fig. 3A, B) support the EIS results, revealing isolated cracks after 24 h of immersion, indicating initial degradation.

Inner layer. A key parameter indicating gradual degradation is the open circuit potential (OCP). The initial OCP value for all formulations was approximately −0.340 ± 0.007 V, consistent with values reported for similar coatings[35]. Over time, the OCP increased towards 0 V, reaching −0.075 ± 0.038 V after 35 days, which is close to the OCP of titanium exposed to aqueous solutions[36]. This shift confirms the gradual degradation of the coatings.

Impedance spectra (Fig. 2C left, 2D left, and 2E left) indicate that all the coatings maintained impedance values in order of 10^5 Ω cm^2 throughout the exposure period, confirming their stability. Analysis of the total system resistance (|Z| at 10^{-2} Ω cm^2) showed an initial increase in barrier properties within the first 7 days, followed by a gradual decrease due to coating degradation.

Despite the presence of drugs, the impedance modulus and phase angle (Fig. 2C right, 2D right and 2E right) exhibited similar behaviour to ControlD, suggesting that dipyridamole incorporation did not introduce additional degradation processes.

The phase angle reflects the capacitive impedance behaviour in the studied frequencies[37]. In these curves (Fig. 2C right, 2D right, and 2E right), there are three different regions can be distinguished depending on the frequency range. High frequencies correspond to the outer coating/electrolyte interphase, medium frequencies are related to the inner interphase of the coating/Ti oxide layer, and lower frequencies register the metal/coating interphase behaviour[38].

In general, the phase angle decreased in the high-frequency region during immersion in all systems, suggesting greater coating capacity due to water absorption. This can be explained by coating damage caused by surface erosion or the creation/appearance of pores and cracks.

Regarding medium frequencies, during the initial hours, phase values increased and then remained constant. This initial behaviour indicates titanium oxide layer formation, where the interphase should be compact and stable during the first few days. The phase angle related to lower frequencies increased for all assays except at 48 h, which may suggest reduced permeability in the metal/coating interphase due to oxide layer formation.

In the bilayer system (Fig. 2E right), the phase angle increased during the first 48 h, then remained constant until day 7, and finally showed a decreasing trend. The initial increase in capacitance could have occurred because the coating was not fully wetted. This is also demonstrated by the displacement of the phase angle towards lower frequencies in the 4–48 h range, indicating an increase in the area exposed to the electrolyte[37]. The progressive decrease from day 7 onwards indicates an increase in capacity due to coating degradation.

At medium frequencies, the phase angle increased during the first 14 days and then remained constant. At low frequencies, the phase angle showed a sharp decrease between 4 and 48 h, then remained almost constant until another increase from day 21 until the end. The initial trend could be explained by the coating not being fully wetted. Up to day 21, an equilibrium was established between coating degradation and oxide layer formation, explaining the relatively stable phase angles in this region. The final increase suggests reduced coating degradation.

Drug release study: antibiotics and dipyridamole release study: HPLC and fluorescence

Figure 3A shows the kinetic drug release profiles of all antibiotic formulations, while Fig. 3B presents the dipyridamole release kinetics.

The antibiotic release data obtained were fitted to a first-order kinetic model with the factor (δ) and an empirical non-ideality parameter (Eq. 1)[39,40]. δ ranges from 0 to 1. When its value is closer to 0, it indicates that most of the payload release occurs at the beginning. Conversely, if the parameter is closer to 1, it implies a purely first-order kinetic release[41]. In Eq. 1, Y represents the percentage of antibiotic released at time t, $Y_{\max}$ is the maximum amount of antibiotic released (in %), and k is the release constant. The equations for each experiment are summarised in Table 3.

$$Y = Y_{\max}(1 - e^{-kt})^{\delta} \tag{1}$$

The dipyridamole release kinetics were determined through fluorescence measurements. Before assessing the released concentration of the compound in each coating over time, the fluorescence intensity for known

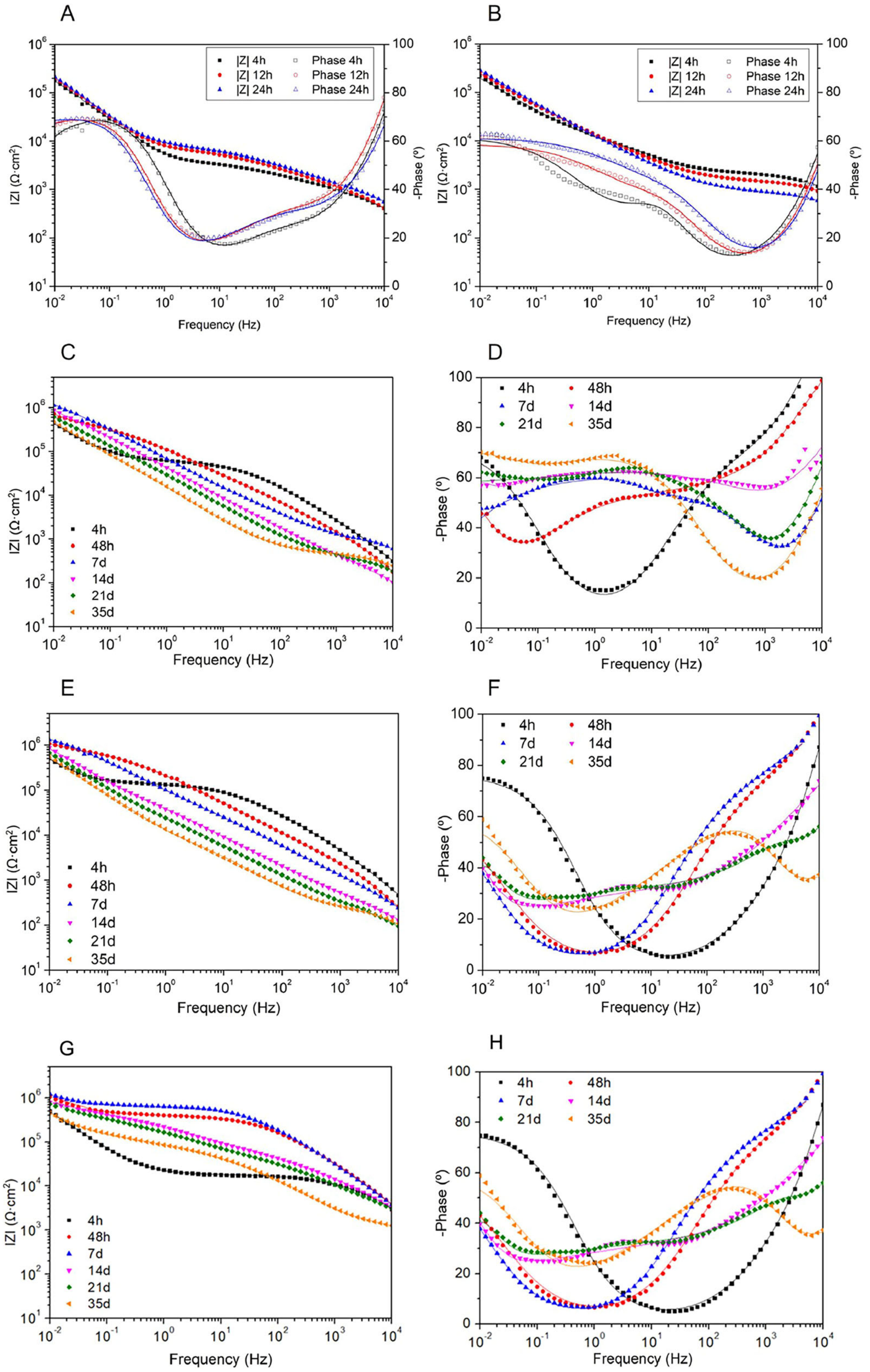

Fig. 2 | Electrochemical impedance spectroscopy analysis of coatings over time. Evolution of Bode spectra over 24 h for outer coatings: **A** ControlA and **B** LNZ-LEV. Evolution of Bode spectra over 35 days for coatings: **C** modulus plot and **D** phase plot of ControlD, **E** modulus plot and **F** phase plot of hc.DIPI, and **G** modulus plot and (**H**) phase plot of bilayer coating. Symbols represent experimental values, while continuous lines correspond to the fitted values from the equivalent circuit.

dipyridamole concentrations was measured within the release range of the coatings. The regression coefficient obtained for the release curve was 0.985. The released quantity of DIPI increased linearly over time ($R^2 = 0.3978$, $p < 0.0001$ for lc.DIPI; $R^2 = 0.8922$, $p < 0.0001$ for mc.DIPI; and $R^2 = 0.7061$, $p < 0.0001$ for hc.DIPI,). The DIPI release rate was 361 ± 19, 408 ± 40.7, 471 ± 68.4 ng/h. Sustained dipyridamole release was also observed in HA/β-TCP scaffolds for up to 240 h[22], demonstrating its stability in different structures and its ability to be released in a sustained manner over time.

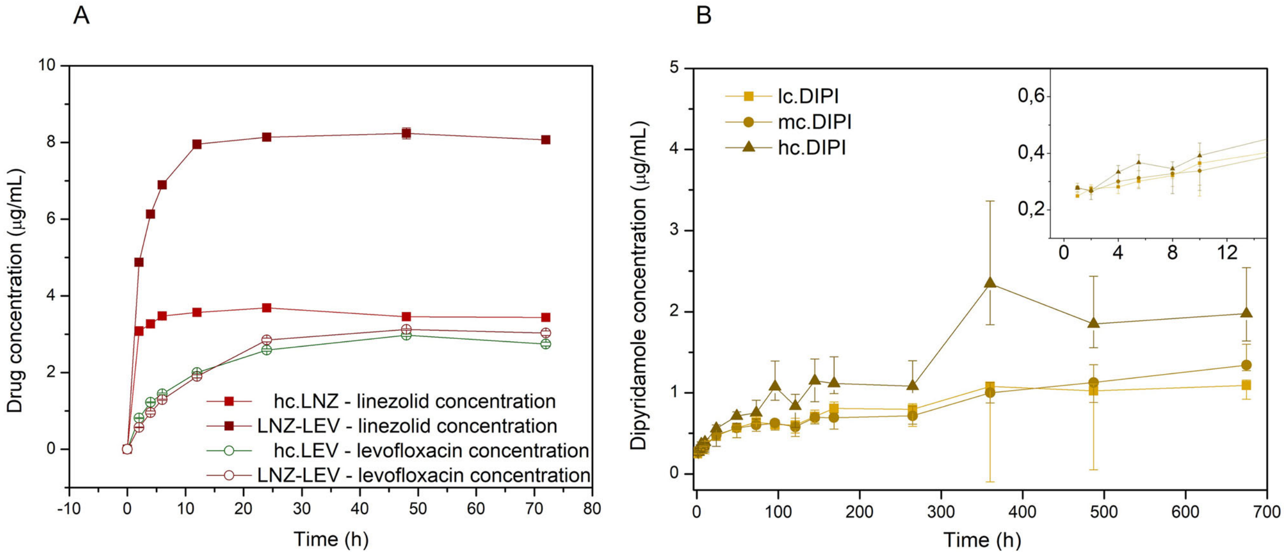

Fig. 3 | Drug release kinetics from antibiotic and dipyridamole-loaded coatings. Kinetic drug release from hc.LNZ, hc.LEV, and LNZ-LEV over time measured by HPLC (**A**), and dipyridamole release kinetics over time measured by fluorescence (**B**). Data are represented as median and interquartile range of the amount of antibiotic measured in three different samples.

Microbiological studies

The MICs and the FIC indices are shown in Table 4. All evaluated strains were susceptible to levofloxacin (MIC < 1 mg/L for staphylococci and *E. coli*, and MIC < 2 mg/L for *P. aeruginosa*). Both staphylococcal strains were susceptible to LNZ (MIC < 4 mg/L). Synergy between LNZ and LEV was only observed in *S. epidermidis*. Our results are in line with those obtained by Giacometti et al., who demonstrated that LNZ combined with LEV and/or vancomycin in a rat subcutaneous pouch model of graft infection caused by *S. epidermidis* with intermediate resistance to glycopeptides resulted in no evidence of staphylococcal infection[41].

In Fig. 4A, B is shown bacterial biofilm and planktonic bacterial concentration, for both staphylococci, loaded coating LNZ-LEV was effective both preventing biofilm formation (more than 99%), and reducing planktonic bacteria generation (more than 74%).

Against *S. aureus* strain, its behaviour demonstrated a synergic effect between both drugs. While isolated, levofloxacin and linezolid reached a biofilm formation prevention around 98.6% and 93%, respectively, and the reduction of 21.1% and 38.5%, respectively, in planktonic bacteria. However, studies with *S. epidermis* strain did not result the same effect although for this strain, it was achieved greater inhibition with all loaded coatings. These differences between *S. aureus* and *S. epidermidis* in terms of inhibition of biofilm development by linezolid and levofloxacin are explained by a greater ability of *S. epidermidis* to develop acquired resistance[42], a greater propensity to form more robust biofilms[43], and genetic resistance to fluoroquinolones and linezolid more pronounced than *S. aureus*[44].

Regarding to Gram-negative bacilli, biofilm formation in both strains was successfully inhibited, achieving 99.9% against *E. coli* and 99.3% against the *P. aeruginosa* strain. Reduction of planktonic bacteria generation was also achieved, resulting in the reduction of 89.8% against *E. coli* and 80.4% against *P. aeruginosa*. These results demonstrate the efficacy of levofloxacin, an antibiotic which has proven to be notably useful to treat infections caused by these two Gram-negative bacteria[45]. The higher performance against *E. coli* compared to *P. aeruginosa* is fully expected considering that the minimum inhibitory concentration for *P. aeruginosa* is almost twice as high as for *E. coli*[45,46] and that, though levofloxacin is effective against *P. aeruginosa*, this bacterium has a greater tendency to develop resistance compared to *E. coli*.

Table 3 | Kinetics drug release equations for each antibiotic in hc.LNZ, LNZ-LEV, and hc.LEV samples

Sol-gel	Equation	R^2
hc.LNZ	$Y = 3.543 \cdot (1 - e^{-0.324t})^{0.195}$	0.7409
LNZ-LEV (LNZ concentration)	$Y = 8.176 \cdot (1 - e^{-0.208t})^{0.488}$	0.9925
hc.LEV	$Y = 2.885 \cdot (1 - e^{-0.075t})^{0.655}$	0.9887
LNZ-LEV (LEV concentration)	$Y = 3.129 \cdot (1 - e^{-0.0842t})^{0.957}$	0.9925

As visual support for these results, samples of the ControlA and LNZ-LEV coatings were taken and subjected to the procedure described for the evaluation of the inhibition of biofilm formation with the four tested reference strains. After incubation for 24 h, the coatings were viewed by SEM and the micrographs obtained are shown in Fig. 4C–F. The images showed a remarkable difference between the bacterial growth developed on the coatings without antibiotic loading and the LNZ-LEV coating. Only the presence of isolated bacteria could be observed in the coating loaded with both antibiotics for all tested strains, apart from the coating in the presence of the *P. aeruginosa* strain, where a higher bacterial growth was observed, although much lower than in the presence of the control coating. The appearance of the biofilm grown on the control and on the LNZ-LEV-loaded sol-gel were remarkable for all bacteria tested. Staphylococci on ControlA showed a biofilm composed of multiple layers of cocci (Fig. 4 C-D), while the few cocci adhered on the antibiotic-loaded sol-gel showed significant damage to their cell wall, e.g., *S. aureus*, or alterations in size, e.g., *S. epidermidis*. These morphological changes in these bacteria would be due to the bactericidal effect of the combination of both antibiotics against *S. aureus* and to the action of linezolid on *S. epidermidis*[47]. On the other hand, the biofilm of Gram-negative bacilli on ControlA showed a large biomass of biofilm growth, while on the sol-gel loaded with LNZ-LEV, *E. coli* grew sparsely as individual bacilli and *P. aeruginosa* showed less abundant and populated microcolonies in comparison to the control. Interestingly, both Gram-negative bacilli showed changes in morphology resulting in larger than normal bacilli (>2 mm long). These morphological changes are directly related to levofloxacin favouring cell elongation due to interference with DNA replication and cell division[47].

Cell studies

Results from cellular studies are presented in Supplementary Fig. 4A, B. Coatings did not showed cytotoxicity although cell proliferation is slightly compromised ($p < 0.05$) maybe due to fluoroquinolones toxicity[45–47].

Table 4 | Thickness and contact angle values for ControlA, hc.LNZ, hc.LEV, LNZ-LEV, ControlD, hc.DIPI, bilayer system and uncoated titanium

Surface	Thickness (µm)	Contact angle (°)
TiPM	–	57.8 ± 5.3
ControlA	12.3 ± 1.1	84.4 ± 2.2
hc.LNZ	12.4 ± 0.9	80.0 ± 1.3
hc.LEV	12.0 ± 1.0	81.3 ± 2.6
LNZ-LEV	12.8 ± 1.6	79.8 ± 2.6
ControlD	9.4 ± 0.5	87.6 ± 2.0
hc.DIPI	9.8 ± 0.7	86.1 ± 2.8
Bilayer	13.0 ± 0.7	87.2 ± 2.5

Cell viability, cell proliferation and bone mineralisation of the dipyridamole-loaded coatings were also evaluated (Fig. 5A–C, respectively). In both cell viability and cell proliferation studies, no statistically significant differences were found in any of the coatings regarding cell control. Although among the osteostimulant feature of these layers, no enhancement of cell proliferation was found, differences in bone mineralisation did as reflected in Fig. 5C where this parameter was significantly increased in hc.DIPI coating compared to the cell control ($p < 0.001$). Average percentage of cell mineralisation in hc.DIPI sample, compared to cell control (normalised to 100%), was approximately 240% after 10 days of culture, results that correlate with previous data, were dipyridamole is able to enhance mineralisation as well as revert the lost induce by other compounds[17,23].

In vivo assay: bilayer system

In vivo assay: animal monitoring. Figure 6 shows the evolution of three behavioural variables over time: weight, limping, and piloerection. These values were recorded from the day mice had surgery until sacrifice time.

All groups gained weight over time, although this gain was greater for the non-infected groups. The weight increase rate was significantly higher in those mice from the control group (324.47 ± 30.05 mg/day) than those in the treatment group (262.08 ± 34.45 mg/day) ($t_{178} = 12.947; p < 0.0001$). This may be due to the linezolid effect which is able to provoke alterations in energy metabolism and the gut microbiota[48]. In the context of infection, those infected mice with a coated implant showed a significantly higher weight increase rate (225.41 ± 34.05 mg/day) than those with an uncoated implant (209.77 ± 18.46 mg/day) ($t_{137.157} = 3.831$, $p = 0.0002$). This difference stems from the efficacy of the preventive antibiotics-loaded sol-gel layer which can reduce locally the bacterial load and favour the weight increase in those animals.

In our in vivo model, limping and piloerection were used to track joint discomfort and widespread malaise, which are frequently linked to infection[49]. Limping decreased significantly over time in all groups. In uninfected groups, the presence of lameness in all mice was eliminated by day 10 for both groups (Fig. 6C). For the *S. aureus*-infected groups, the coated group achieved a total decrease in limping from day 30, however, the untreated group had limping until the end of the study, meaning at least two mice remained lame. (Fig. 6D). In mice with uninfected implants, piloerection showed no significant variation over time ($p > 0.05$) (Fig. 6E). Piloerection in groups with *S. aureus* infection showed a significant decrease over time ($\rho = -0.8814, p < 0.0001$ for group of mice with uncoated implant and $\rho = -0.9345$, $p < 0.0001$ for those mice with sol–gel coated implant). Within these groups, the treatment group achieved complete elimination of piloerection at the day 30 of the study, while control group did not (Fig. 6F). These results are consistent with a previous study which demonstrated that the sooner the limping and piloerection disappear, the lower the bacterial load in the femur with the infected implant[26].

In vivo assay: microbiological results. Figure 7D presents number of colonies forming units found per femur gram from the infected groups (group 3 Control Infection, $n = 6$ and group 4 Treatment Infection, $n = 6$). One hundred percent of the mice in the group of infected mice with uncoated implants had a positive *S. aureus* culture, while 33.33% of the animals infected with coated implants had a negative culture (2/6). The difference between the two groups was statistically significant ($p < 0.01$). These results are in line with our previous study where we demonstrated that a moxifloxacin-loaded sol–gel coating a similar implant was able to inhibit completely the development of infection in the same in vivo model[26].

Figures 7D, E shows bone mineral content (BMC) graphs and femur bone mineral density (BMD) of uninfected groups (group 1 Control and group 2 Treatment) differentiated by bone regions. In both BMC and BMD, statistically significant differences ($p < 0.05$) were found between the groups of mice with coated and uncoated implants. In all regions, except for the proximal epiphysis, where the implant was not located, an increase in both BMC and BMD were found in treatment groups. Similar results were found in calvaria critical size defects, were collagen sponges or HA/β-TCP scaffolds coated with dipyridamole induced new bone regeneration[17,18,22]. The data shown in this manuscript, confirm the previous data were combining the capacity of ceramic scaffolds with the osteoinductive qualities of dipyridamole was indicated for critical size defects. Herein we demonstrate that the combination of an antibiotic with dipyridamole is promoting even a better bone regeneration that any of the compounds alone.

In vivo assay: histologic study. Figure 8 shows a representative images selection of femur longitudinal sections from the uninfected, Control and Treatment groups after different dying procedures. When comparing both implants, it was observed that those which contained dipyridamole demonstrated new bone formation increase in the surrounded are of the implant, principally in condyles area. The number of TRAP-positive cells decreased in the presence of dipyridamole, as did the number of CD68-positive cells (which are markers of macrophages). Increased dyeing in both bone remodelling markers, ALP and cathepsin K, were also observed. When we compared these results with our previous data in calvaria critical size defects[22], we observed that dipyridamole exerts the same osteogenic effect in both systems. This indicates that although the type of bone in both bones is different, similar mechanisms are involved, and dipyridamole-coated scaffolds is also compelling in treatment of long bones defects.

Conclusions

Biofunctionalizations of the outer layer was successfully achieved with linezolid and levofloxacin as well as with the inner layer. The loaded concentrations were 2.46 mg/ml linezolid, 1.84 mg/ml levofloxacin, and 1.25 mg/ml dipyridamole. The antibacterial outer layer loaded with linezolid and levofloxacin was able to inhibit biofilm development and planktonic growth of both Gram-positive and Gram-negative bacteria for at least the first 24 has demonstrated in the in vitro assays. The osteostimulating inner layer, loaded with the highest concentration of dipyridamole, was able to increase in vitro mineralisation. The bilayer system was able to significantly reduce symptoms and bacterial load in the femur of *S. aureus*-infected mice with coated implants and increase bone metabolism in the immediate bone in contact with the implant, resulting in an increase in bone mineral content and bone density in vivo.

Methods

Preparation of the inner layer formulation

For inner layer biofunctionalisation, dipyridamole was chosen.

The osteoinductive layer coating was prepared by sol–gel technology. Methyl-trimethoxysilane (MTMOS, 95%, Sigma Aldrich, St. Louis, MI, USA) and tetraethyl orthosilicate (TEOS, 98%, Sigma Aldrich) were selected as precursors for the synthesis. Ethanol was used in stoichiometric

Fig. 4 | Bacterial biofilm formation on coatings. Bacterial biofilm concentration per area unit (CFU/cm^2) (**A**) and planktonic bacterial concentration (ABS) (**B**) of *S. aureus*ATCC 29213, *S. epidermidis* ATCC 35984, *E. coli* ATCC 25922, and *P. aeruginosa* ATCC 27853 on coatings: ControlA, hc.LNZ, hc.LEV, and LNZ-LEV. Error bars represent the interquartile range. *$p < 0.05$, **$p < 0.01$, ***$p < 0.001$ (Wilcoxon test). Backscattered electron SEM micrographs of coating surfaces after 24 h of bacterial incubation: (left) ControlA and (right) LNZ-LEV, showing the biofilm in *S. aureus*, *S. epidermidis*, *E. coli* and *P. aeruginosa* in panels (**C**, **D**), (**E**, **F**), (**G**, **H**), and (**I**, **J**), respectively.

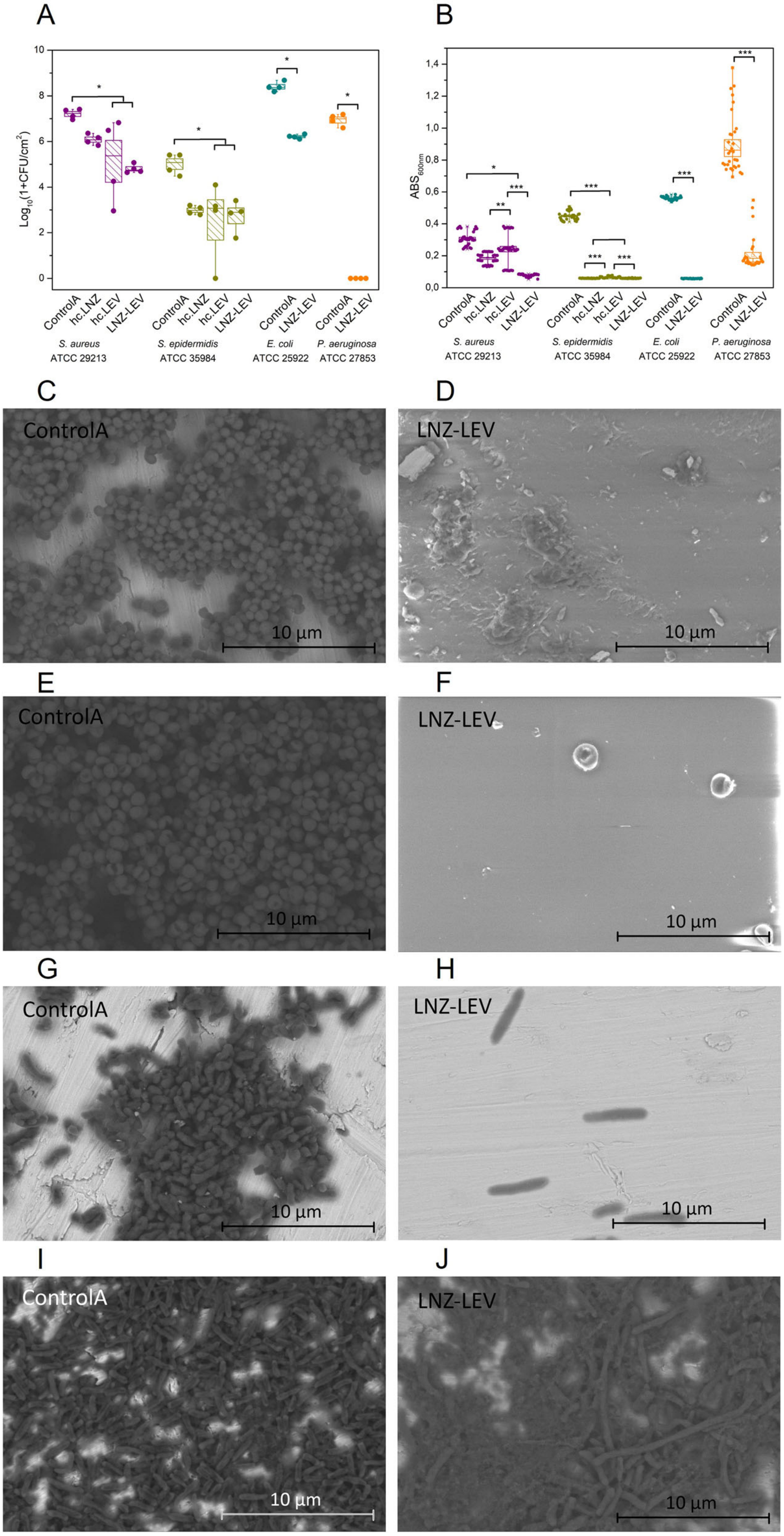

relation with the precursors, saving 6 mL for dissolving dipyridamole. The solution was then magnetically agitated. The dipyridamole solution was prepared in a separate container using deionised water (acidified until pH = 1.2 with HNO_3 to accelerate hydrolysis), in stoichiometric relation, and the stored ethanol. The stability of dipyridamole in an acidic medium has been investigated in various studies[50–52], which report that it remains stable under the conditions used in our study. Dipyridamole is soluble in organic solvents such as ethanol, DMSO, and dimethylformamide (DMF), with solubilities of approximately 5 mg/mL in ethanol and 30 mg/mL in DMSO and DMF. However, it exhibits poor solubility in aqueous solutions. Its molecular weight is 504.63 g/mol[53]. The prepared dipyridamole solution was added at an approximate rate of 1 drop

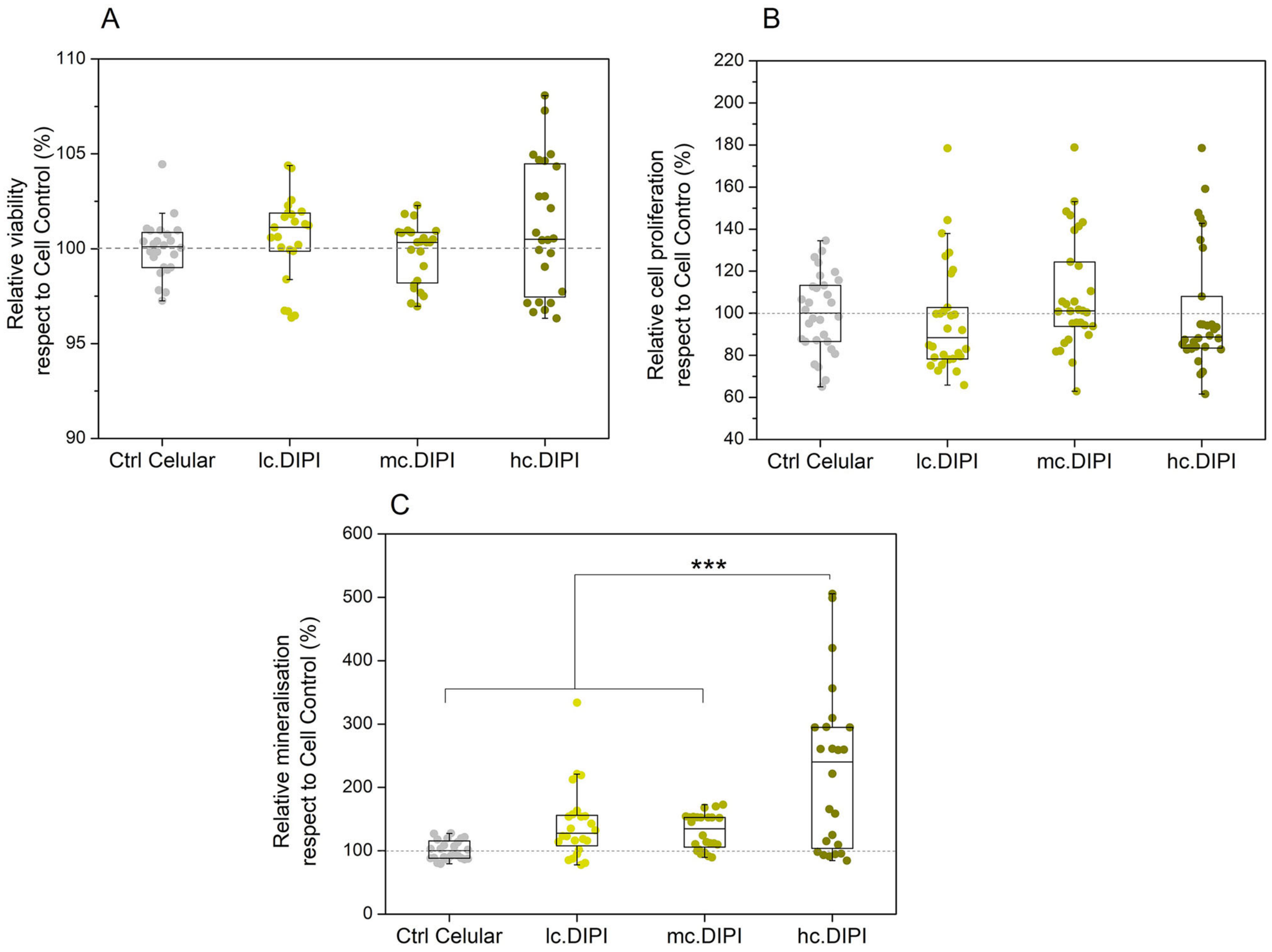

Fig. 5 | Biocompatibility and mineralization of sol-gel coatings. Cell viability (**A**) and cell proliferation (**B**) at 48 h, and mineralisation at 240 h (**C**) of MC3T3-E1 cells without treatment (Cell Control) or treated with sol-gel lc.DIPI, mc.DIPI, or hc.DIPI. Data are represented as median and interquartile range in 32 biological replicates. ***$p < 0.01$ by Wilcoxon test for independent samples.

per second to the precursor solution. Finally, the synthesis was magnetically agitated for 2 h at 150 rpm.

Regarding the dipyridamole concentrations selected, three formulations were prepared: lc.DIPI (0.63 mg/mL), mc.DIPI (0.94 mg/mL), and hc.DIPI (1.25 mg/mL), plus another sol–gel named ControlD without any drug. Once the synthesis was concluded, sols were deposited onto metallic substrates of powder-metallurgical titanium (TiPM). Dip coating was performed at 100 mm/s using the KSV DC equipment (Biolin Scientific, Västra Frölunda, Sweden). Finally, coatings were dried at 80 °C for 2 h.

Preparation of the bilayer system

The bilayer system comprised an outer layer biofunctionalised by a combination of antibiotics and an inner layer (explained in this article). The outer (antibiotic) layer was synthesised following the procedure described by Toirac et al.[10]. These coatings were synthesised from methacryloxypropyltrimethoxysilane (MAPTMS, 98%, Acros Organics, Thermo Fisher Scientific, Waltham, MA, USA) and tetramethyl orthosilane (TMOS, 98%, Acros Organics), with a 1:2 molar ratio as described by Hadad et al.[15]. An organophosphorus compound, tris(tri-methylsilyl) phosphite (92%, Sigma Aldrich, St. Louis, MI, USA), was added to the sol in a molar ratio of 1:50 (silanes:organophosphorus compound) to enhance cellular proliferation, as demonstrated in prior studies[13]. Ethanol was added as a solvent to avoid phase separation and water was used as a reagent to initiate the hydrolysis reaction, both were added in stoichiometric amounts. After the addition of water, the suspensions were stirred for 24 h in a glove box. The loading of antibiotics is explained in Table 5.

As shown, the coating was biofunctionalised using two different antibiotics separately: levofloxacin (LEV, Sigma Aldrich) and linezolid (LNZ, 98%, Acros Organics). The goal was to increase the antibacterial spectrum to target both Gram-positive cocci and Gram-negative bacilli species. The combination of the drugs, rather than monotherapy, aimed to: (1) increase the spectrum to fight against all potential pathogens, (2) prevent the development of resistance and, (3) achieve the synergistic action of the combination against *S. epidermidis* and/or the medication of polymicrobial infections that may not be treatable with a single drug[53–58].

Once the synthesis was completed, the inner layer was first deposited as explained in Section "Synthesis characterisation of sols and xerogels: outer and inner layer". Afterwards, the outer layer sols were deposited over the inner layer by dip-coating (KSV DC, Biolin Scientific, Västra Frölunda, Sweden) at 200 mm/s and dried at 60 °C for 1 h.

Characterisation of sol–gel synthesis: outer and inner layers

The hydrolysis and condensation reactions involved in the synthesis were monitored by Fourier Transform Infrared Spectroscopy (FT-IR). Each sample was prepared by depositing one drop of the sol–gel formulation on a pressed KBr disc. Spectra were recorded using the Thermo Scientific NICOLET iS50 FTIR (Thermo Fisher Scientific, Waltham, MA, USA) at room temperature in absorbance mode, covering the mid-infrared range from 400 to 4000 cm^{-1}, with a resolution of 4 cm^{-1} and a 0.1 cm^{-1} range, by performing 10 scans. For each sol–gel synthesis, three measurements were carried out.

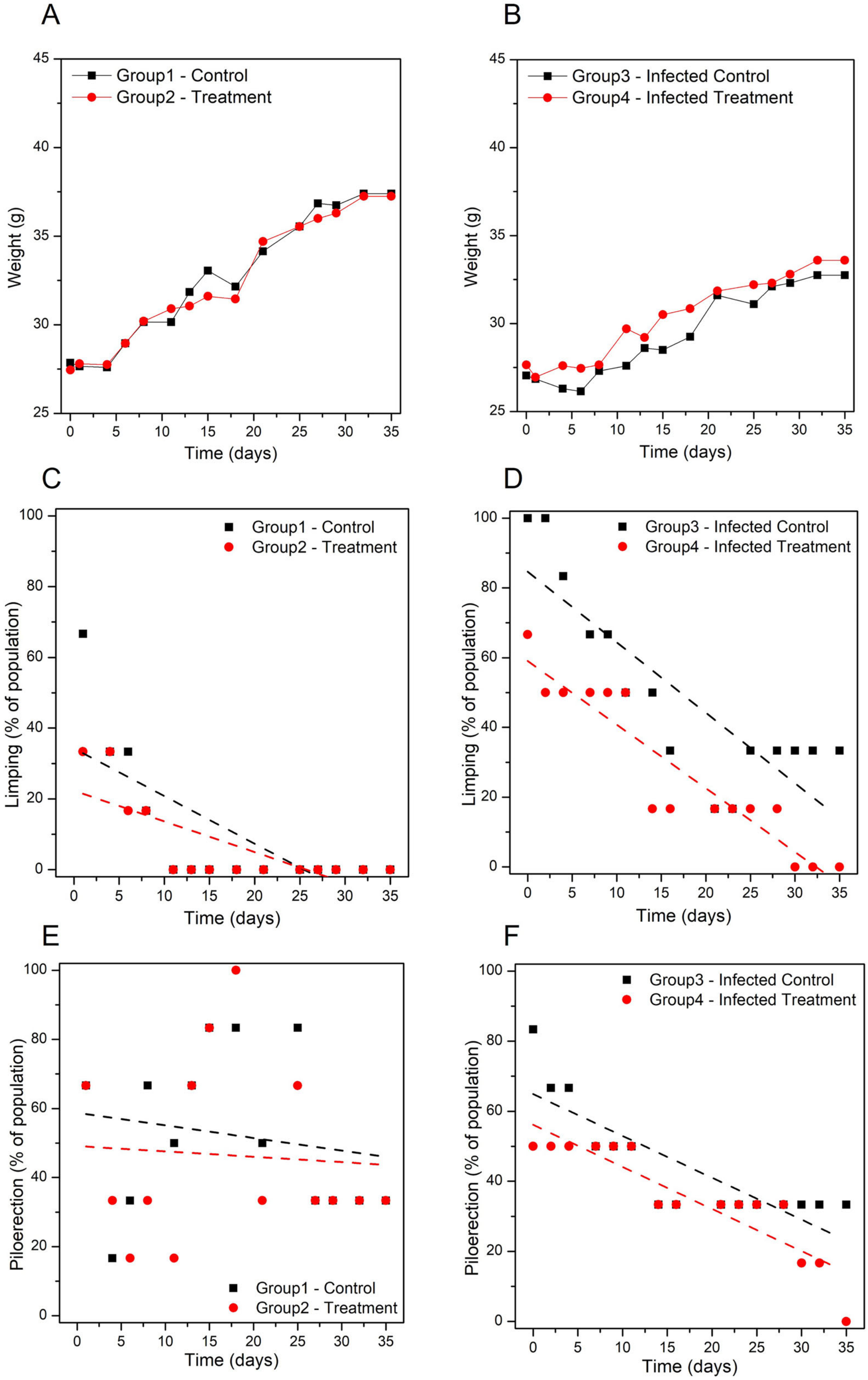

Fig. 6 | Physiological response to implant coatings in vivo. Median weight (**A**, **B**), limping incidence (**C**, **D**), and piloerection (**E**, **F**) in groups with uncoated (black square) and coated (red circle) implant insertion over time. The dashed lines represent the trend of the data. $^{**}p < 0.01$ by Wilcoxon test for independent samples.

Characterisation of xerogel: outer and inner layers

Sols were dried at 60 °C for 4 h and ground in an agate mortar prior to nuclear magnetic resonance spectroscopy of silicon nuclei (^{29}Si-NMR). ^{29}Si-NMR was performed in a Bruker AVANCE 400 spectrometer (Bruker, Billerica, MA, USA) equipped with a fast Fourier transform unit. The frequency used during the measurements was 79.48 MHz (9.4 T). Samples were spun at 10 kHz around an axis tilted 54°44′ in reference to the external magnetic field. Spectra were recorded with a pulse length of 5 μs (90° pulse), a relaxation delay of 10 s was used, and 6000 accumulations were acquired. Spectra were referenced to tetramethylsilane (TMS).

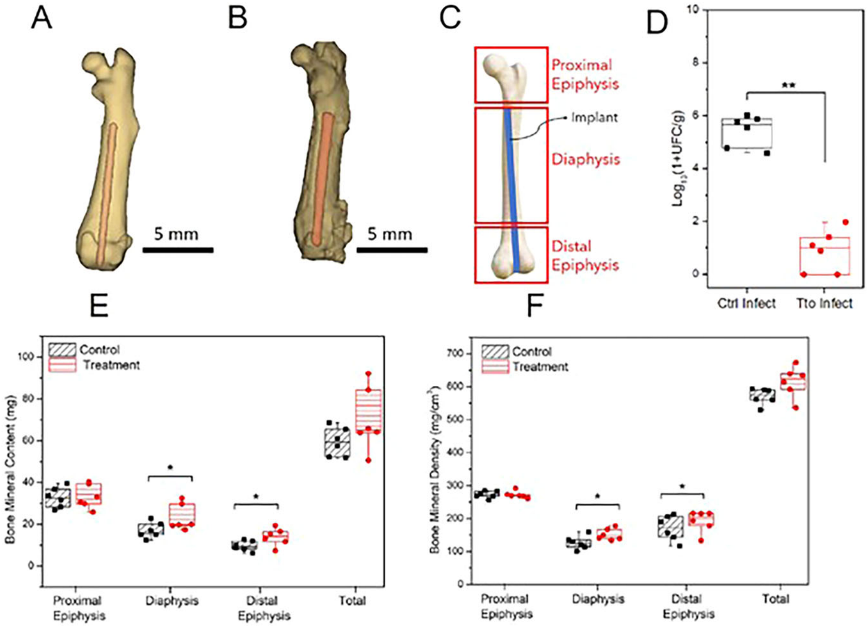

Fig. 7 | Histologic study and bacterial load in bone tissue. Three-dimensional reconstructions of a representative femur sample from the Control group (**A**) and the Treatment group (**B**). Schematic representation of the main regions of the femur and the implant location (**C**). Colony-forming units per gram (CFU/g) of femur from each group of mice (**D**) in uninfected (left column) and Sa5-infected (right column) conditions. Bone mineral content (**E**) and bone mineral density (**F**) of Control and Treatment groups without infection. Data are represented as median and interquartile range. *$p < 0.05$ by Wilcoxon test for independent samples.

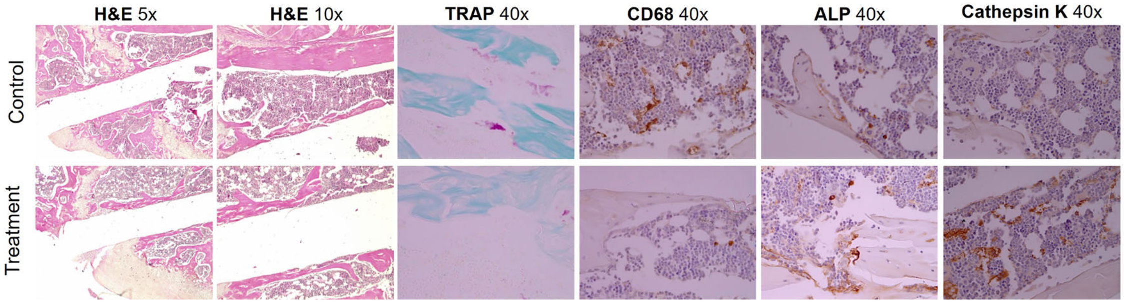

Fig. 8 | Immunohistochemistry for different bone cells markers. Representative images dyed for haematoxylin–eosin (H&E), tartrate resistant acid phosphatase (TRAP) dyed, macrophages (differentiation group 68, CD68), alkaline phosphatase (ALP) and cathepsin K (cath. K). All H&E and immunostaining images were taken at 40× magnification.

Physicochemical characterisation: each layer and bilayer system

Surface morphology and coating composition were evaluated by scanning electron microscopy (SEM) using the FEI Teneo instrument (FEI Company, Hillsboro, OR, United States) equipped with a W filament. The lateral area and the underside of the samples were covered with a Cu tape to ensure conductivity. Images were taken at low vacuum applying 2–5 kV and 0.2 nA.

Topography was studied using atomic force microscopy (AFM), performing scans of area sizes 5×5 and 40×40 μm^2 with a resolution of 512×512 pixels. The AFM instrument was the Park XE-150 system (Park Systems Corp., Suwon, South Korea), used in non-contact mode under room conditions at a scanning frequency of 0.3 Hz. The silicon cantilever tip chosen (N-type, μmasch, Tallinn, Estonia) had a nominal radius of 8 nm. Surface roughness analysis and image processing were carried out with XEI software version 4.3.0 (Park Systems Corp.).

Coating adhesion was qualitatively evaluated by crosscutting using ASTM D 3359-02 (Standard Test Methods for Measuring Adhesion by Tape Test, Test Method B, Cross-cut Tape Test) as a ref. 8. This test involves making incisions that reach the titanium substrate, both parallel and perpendicular, forming squares of equal size. A standardised tape is applied to this cut, which is then peeled off. By assessing the percentage of the surface without coating, a classification is made accordance to the standard.

Wettability was determined by contact angle measurements on the Dataphysics OCA 20 automatic goniometer (DataPhysics Instruments GmbH, Filderstadt, Germany). A 3 μL drop of phosphate-buffered saline (PBS, Sigma Aldrich) was deposited at 1 μL/s on the coating surface (at room temperature). The values were calculated by averaging nine measurements corresponding to three different points for three samples of each formulation.

Layer thickness was measured using a Neurtek ultrasonic thickness gauge (Neurtek Instruments, Eibar, Gipuzkoa, Spain). The values shown are the result of at least 6 measurements on different samples per formulation.

Coating degradation study: each layer and bilayer system

The degradation of the synthesised coatings was evaluated using a Metrohm Autolab PGSTAT302N potentiostat/galvanostat (Metrohm AG, Herisau, Switzerland). A conventional three-electrode configuration was used, with the working electrode being the titanium substrate (TiPM) coated, the reference electrode as Ag/AgCl/KCl ($E = 0.197$ V vs. NHE), and the counter electrode as a platinum wire. The electrolyte consisted of a PBS solution (Sigma Aldrich) at 37 ± 1 °C. Water recirculation at 37 °C in a glass cell was carried out by the Julabo HC/F30 thermostatic circulating bath with heating (JULABO UK Ltd., Stamford, UK).

Samples were prepared before immersion in the electrolyte by placing a copper electrical contact on the metal without any coating. Afterwards, the cable-attached face and edges of the sample were covered with an edge-retention lacquer (MacDermid ref. 166054,65415). The measuring area was 1 cm^2.

The sinusoidal perturbation chosen was ±10 mV relative to the open-circuit potential (OCP), and sweeping a range from 10 mHz to 10 kHz, taking 10 points per decade. For the outer layer, measurements were taken at regular 2-h intervals for 24 h. In contrast, inner layer measurements were performed at 4, 48, 168, 336, 504, and 840 h. All samples were evaluated at least three times using three formulation-coated replicates inside a Faraday box to avoid interference. Before and after each impedance measurement, the OCP was recorded.

Impedance spectra were obtained and analysed using Nova v2.1.4 (Metrohm AG) and Z-view v3.3e (Scribner Associates, Charlottesville, VA, USA) software, respectively.

Drug release study: outer and inner layers

For the outer layer, in a 6-well Transwell® plate (Corning, NY, USA) with a 0.4 µm filter, 500 µL of the sol–gel of each antibiotic-loaded formulation (minimum volume to cover the well bottom) was deposited after 2 h of synthesis. These plates were dried in a laminar flow hood overnight. Once the sol–gels were dried, they were exposed to 3 mL of PBS (Sigma Aldrich) at 37 °C. Aliquots of 50 µL were collected at different time points (2, 4, 6, 12, 24, 48, and 72 h), then replaced with fresh deionised water and stored at −80 °C until analysis. Antibiotic concentrations were determined by a validated HPLC method, using ultra-high-performance liquid chromatography-tandem mass spectrometry (UHPLC–MS/MS)[59].

For the inner layer, fluorescence measurements were recorded on the EnSpire Multimode Plate Reader instrument (Perkin Elmer, Waltham, MA, USA). In a 6-well Transwell® plate (Corning, NY, USA) with a 0.4 µm filter, 500 µL of the sol–gel of each DIPI-loaded formulation (minimum volume to cover the well bottom) was deposited after two hours of synthesis. These plates were dried in a laminar flow hood overnight. Once the sol-gels were dried, they were exposed to 3 mL of PBS (Sigma Aldrich) at 37 °C. Aliquots of 300 µL were taken at each time point and transferred to a 96-well plate to measure dipyridamole fluorescence at an excitation wavelength of 413 nm and an emission wavelength of 500 nm[60]. The same volume was replaced with fresh PBS. Measurements were taken at different times (1, 2, 4, 6, 8, 10, 24, 48, 72, 96, 120, 144, 168, 264, 360, 480, and 672 h). The drug concentration for fluorescence values obtained was calculated based on the calibration curve performed previously. Calibration was performed by varying the drug concentration between 120 µg/mL and 0.058 µg/mL. The concentration of each sample was then normalised, considering the dilution and the corresponding calibration curve. The aliquots taken and the plate were stored in a light-protected environment.

Microbiological characterisation: minimal inhibitory concentration and synergy between the antibiotics chosen

Determinations of the minimal inhibitory concentrations (MIC) by the E-test were performed according to the manufacturer's recommendations. The concentration range was 0.016–256 g/ml for linezolid and 0.002–32 g/ml for levofloxacin (Biomérieux, France). The inoculum was matched to a McFarland standard of 0.5 in sterile saline, and then, with a cotton swab, a lawn of bacteria was created on the Mueller-Hinton agar plates (Biomérieux, France). The plates were incubated for 20 h at 37 °C and 5% CO_2. The MIC was interpreted as the value at which the inhibition zone intersected the scale on the E-strip.

The synergy between linezolid and levofloxacin was determined using the methodology previously described by White et al.[61]. For this purpose, the inoculum and streaked Mueller–Hinton agar plates were prepared as previously described. The E-test strips were placed on the Mueller–Hinton agar in a cross formation, with a 90 angle at the intersection between the scales at their respective MICs for the organism. The plates were incubated for 20 h at 37 °C and 5% CO_2. After incubation, the zones of inhibition were read as described above for the determination of the MIC by the E-test. The fractional inhibitory concentration (FIC) index was used to quantify the interaction between linezolid and levofloxacin.

Regarding two antibiotics, A and B, functioning separately or jointly:

$$\text{FIC Index} = (\text{MIC}_{A+B}/\text{MIC}_A) + (\text{MIC}_{B+A}/\text{MIC}_B)$$

where the MIC values of each antibiotic and the antibiotic individually are represented by MIC_A and MIC_B, respectively. The MIC of the first antibiotic plus the second one is denoted by MIC_{A+B}, while the MIC of the second antibiotic plus the first one is denoted by MIC_{B+A}. The FIC index is the sum of FIC_A and FIC_B. A FICI ≤ 0.50 points out synergy, an FICI between 0.50 and 1.00 represents an additive effect, an FICI from 1.00 to 2.00 was defined as indifference, and an FICI greater than 2.00 represents antagonism[62].

Microbiological characterisation: inhibition of biofilm formation assay

The inhibition of biofilm formation was evaluated at the Department of Microbiology of the Fundación Jiménez Díaz Health Research Institute (Instituto de Investigación Sanitaria Fundación Jiménez Díaz, IIS-FJD). The study was carried out with reference strains *S. aureus* ATCC 29213, *S. epidermidis* ATCC 35984, *E. coli* ATCC 25922, and *P. aeruginosa* ATCC 27853. These species represent the most common pathogens associated with implant-related infections and serve as examples of strains susceptible to these antibiotics[2,7].

All strains were stored frozen at −80 °C until experiments were conducted. They were then maintained at 37 °C on tryptic soy agar supplemented with 5% sheep blood (TSS, BioMérieux, Marcy-l'Étoile, France). The day before each test, the corresponding strain was spread onto a new TSS plate to be incubated overnight at 37 °C and 5% CO_2. Each test was performed with four independent cultures.

The protocol followed in this trial is described below:

(1) Coated titanium substrates were placed individually in each 6-well plate (Sigma Aldrich), and 5 mL of a diluted solution of the corresponding strain in tryptic soy broth (TSB, Sigma Aldrich) supplemented with 1% glucose (w/v) was added to achieve a final concentration of 0.5 McFarland (approximately 10^8 colony-forming units, CFU/mL). The plates were incubated at 37 °C and 5% CO_2 for 24 h. After incubation, the parts were washed with sterile 0.9% NaCl saline (SS, B. Braun, Melsungen, Germany).

(1.1) Coatings were scraped with sterile, halved tongue depressors. These were placed in 50 mL Falcon™ conical tubes (Thermo Fisher Scientific) with 5 mL of SS and sonicated at room temperature for 5 min[63]. Subsequently, CFU/cm^2 values were estimated using the plate drop method[64].

Table 5 | Antibiotic susceptibility (mg/L) of the different strains used in this study against LNZ and LEV alone or in combination

Strain	MIC_{LNZ}	MIC_{LEV}	$\text{MIC}_{\text{LNZ+LEV}}$	$\text{MIC}_{\text{LEV+LNZ}}$	FIC index	FIC index interpretation
S. aureus ATCC 29213	0.75 (S)	0.125 (I)	0.75	0.125	2	Indifference
S. epidermidis ATCC 35984	0.5 (S)	0.125 (I)	0.125	0.032	0.5	Synergy
E. coli ATCC 25922	>256 (R)	0.64 (I)	ND	ND	ND	ND
P. aeruginosa ATCC 27953	>256 (R)	1 (I)	ND	ND	ND	ND

S susceptible, *I* intermediate or susceptible to high-concentration treatment, *R* resistant. *Note: the phenotype was determined using the EUCAST Clinical Breakpoints (v 15.0). ND* not determined.

(1.2) Non-adherent planktonic bacteria remaining in the incubation medium were quantified by absorbance at 600 nm in eight replicates, using TSB medium alone as a negative control. Absorbance measurements were taken with the EnSpire Multimode Plate Reader (Perkin Elmer).

Data are expressed as median and interquartile ranges for at least three samples. Some of the coatings were observed by SEM after biofilm formation. For this observation, bacteria were fixed with 2.5% glutaraldehyde for 24 h and dehydrated by subjecting them to ethanol concentrations from 10% to 100%, with 10-min intervals at each concentration.

Microbiological characterisation: cell studies: cellular viability, cellular proliferation, and bone mineralisation: outer and inner layers

Cell studies were performed at the Department of Rheumatology and Bone Metabolism at IIS-FJD. The viability of MC3T3-E1 cells was determined following the protocol outlined below:

1. Cells were seeded at a concentration of 10,000 cells/cm^2 in 96-well plates containing α-minimum essential medium with 10% fetal bovine serum and 1% penicillin–streptomycin (αMEM, Invitrogen, Thermo Fisher Scientific) and incubated at 37 °C and 5% CO_2 overnight. After cell attachment, the medium was replaced with αMEM containing 50 mg/mL ascorbic acid (Sigma Aldrich) and 10 mM ß-glycerol-2-phosphate (Sigma Aldrich) to promote osteoblastic differentiation.
2. The tips of MBECTM Biofilm Inoculator (Innovotech, Edmonton, Canada) plate coverslips were coated by dipping them into wells of a 96-well plate containing 200 µL of each sol–gel formulation ($n = 32$ wells per formulation). As a negative control, some wells were left unfilled. The lid tips were dried for 24 h at room temperature. The coating of the plugs on the Calgary device plate allows for the evaluation of the effect of the molecules resulting from the hydrolysis of the sol–gel. This methodology simulates the potential effect of these molecules when they result from the hydrolysis of the sol–gel coating an implant placed inside a bone.
3. The 96-well plates from step 1 were sealed with the lids from step 2 and incubated for 48 h at 37 °C and 5% CO_2. For the determination of cell matrix mineralisation, this incubation was extended for 10 days, replacing the medium every 48 h. After incubation:

a. Cell viability was assessed using the CytoTox 96® non-radioactive cytotoxicity kit (Promega, Madison, WI, USA). Absorbance was measured at 492 nm on the Tecan Infinite 200 Reader instrument (Tecan Group Ltd., Männedorf, Switzerland).
b. Cell proliferation was determined by adding 10% (v/v) AlamarBlue® solution (BIO-RAD, Hercules, CA, USA) to the cell culture, following the manufacturer's instructions. Fluorescence intensity was measured at excitation and emission wavelengths of 540 nm and 600 nm, respectively, using a Tecan Infinite 200 reader (Tecan Group Ltd., Männedorf, Switzerland).
c. Cell matrix mineralisation was measured by staining with Alizarin Red S (Sigma Aldrich). The stain was dissolved with 10% cetylpyridinium chloride in 10 mM sodium phosphate at pH 7. Absorbance was measure at 620 nm using the EnSpire Multimode Plate Reader instrument (Perkin Elmer).

Microbiological characterisation: animal model-based design: bilayer system

The in vivo study was performed using male SWISS RjOrl:SWISS (CD1®) mice, provided by Janvier Labs (Le Genest-Saint-Isle, France), weighing between 20 and 30 g. The surgical interventions were carried out at the facilities of the Animal Research and Experimental Surgery Service at IIS-FJD, in accordance with the provisions of Royal Decree 118/2021, and with the approval of the Animal Protection Area of the Department of Environment, Local Administration, and Territorial Planning of the Comunidad de Madrid (PROEX 111/16).

In this study, a clinical *S. aureus* strain (Sa5), isolated at the Clinical Microbiology Service at IIS-FJD from a 62-year-old male with an acute hip prosthesis infection, was used. *S. aureus* was selected because it is the microorganism most commonly associated with acute PJIs infection[2].

Titanium (Ti6Al4V) implants were prepared from 0.6 mm diameter Kirschner needles supplied by Depuy Synthes (Johnson & Johnson, New Brunswick, NJ, USA). Each needle was cut into implants of 1 ± 0.05 cm in length, then chemically polished as described by Arenas et al.[24] to match surface appearance typically used in clinical practise. Finally, the implants were coated by immersion in sol-gel formulations: first, in the inner formulation (dried for 2 h at 80 °C) and then in the outer formulation (dried for 1 h at 60 °C).

In this study, 16-week-old mice were assigned to four groups: (1) non-coated implants (group 1 Control, $n = 6$), (2) bilayer-coated implants (group 2 Treatment, $n = 6$), (3) *S. aureus* Sa5-induced infection (group 3 Infection Control, $n = 6$) and (4) bilayer-coated implants plus *S. aureus* Sa5-induced infection (group 4, Treatment Infection, $n = 6$). Implant infection in groups 3 and 4 was carried out before surgery, following a modified methodology described by Garlito-Díaz et al.[25]. In this procedure, 1 mL of a 0.5 McFarland inoculum of the Sa5 strain, diluted 10-fold in sterile saline (B. Braun), was incubated with each implant in a 12-well plate at 37 °C and 5% CO_2 for 120 min.

Surgery for the in vivo model followed a model described by Aguilera-Correa et al.[26]. Mice were anaesthetised by inhalation of 3.5% isoflurane. The surgical field was prepared by shaving the skin and disinfecting it with alcohol-based chlorhexidine. The surgical site was isolated using sterile fenestrated drapes. An incision was made over the right knee to access the distal right femur, and the 1 cm implant was inserted. After the procedure, the area was dried with sterile gauze, and the incision was closed[64].

Post-intervention, pain and stress in the animals, as well as their weight, were monitored every 48 h during the week to ensure their physical condition. Pain and stress were evaluated based on the presence or absence of six behaviours linked to this species and the surgery procedure: limping, piloerection, lack of grooming, wound presence, passivity, and aggressiveness. In cases of sustained weight loss, measures were taken to encourage the animals to eat. Five weeks after surgery, the animals were euthanised using hypercapnia, and the entire femur was then retrieved via sterile preparation of the knee, including isolation of the surgical field.

Femurs from infected groups were crushed with a hammer and immersed in 2 mL of saline, then sonicated at 22 °C for 5 min. The resulting inoculum was diluted through a series of 10-fold dilutions and seeded on blood-chocolate agar plates (bioMérieux, France) using the plate spreading method. Bacterial concentration was estimated as CFU/g of bone and adnexa.

Bone samples from each non-infected group were fixed in 10% formaldehyde (VWR Q-Path Chemicals, Avantor Inc., Radnor, PA, USA) for 48 h at 4 °C. The samples were then dehydrated in 96% ethanol for 48 h (renewing ethanol every 24 h) and in 100% ethanol for 48 h (renewing ethanol every 24 h). Finally, they were stored in 100% ethanol until processing.

Three-dimensional computed microtomography was performed using a CompaCT scanner (SEDECAL, Madrid, Spain). Data were collected with 720 projections during a 360° scan, using a integration time of 100 ms with three frames, a photon energy of 50 KeV and a current of 100 µA. Imaging time was 20 min per scan. Three-dimensional representations were generated from the original volumetric images reconstructed by MicroView software (GE Healthcare, Boston, MA, USA). Comparable regions of interest, consisting of three metatarsal joints from each mouse, were selected for analysis. Bone volume (BV, cm^3), bone mass (BM, mg), and bone mineral density (BMD = BM/BV, mg/cm^3) were quantified from micro-CT scans using GE MicroView version 2.2 software.

Samples observed by computed microtomography were acquired for decalcification in 10% EDTA (pH = 7.4) for 4 weeks, following by infiltration in paraffin. Implants were then removed and cut into 5 µm longitudinal sections. Tartrate-resistant acid phosphatase (TRAP) staining was performed using a homemade TRAP buffer (0.1 M acetate buffer, 0.3 M sodium tartrate phosphate, 10 mg/mL Naphtol AS-MX, 0.1% Triton X-100, and 0.3 mg/mL Fast Red Violet LB (Sigma-Aldrich, St. Louis, MO, USA[21]). Briefly, the samples were deparaffinised and incubated in 0.2 M acetate buffer (pH = 5.0) for 1 h. The samples were then incubated in TRAP buffer for 30 min and counterstained with Fast Green.

Immunochemical analysis was performed as described by Mediero et al.[21]. Briefly, sections were incubated with proteinase K solution (20 μg/mL in TE buffer, pH = 8.0) for 15 min at 37 °C on order to recover antigens after deparaffinisation and rehydration. Non-specific binding was blocked with PBS containing 3% BSA and 0.1% Triton X-100 for 1 h, and primary antibodies against cathepsin K (1:25), CD68 (1:200), and alkaline phosphatase (ALP) (1:200) (all from Santa Cruz Biotechnology, Dallas, TX, USA) were incubated overnight at 4 °C in a humidifying chamber. Secondary antibodies (goat anti-rabbit HRP (1:2000), goat anti-mouse HRP (1:2000) (Merck Life Science S.L.U., Madrid, Spain)) were incubated for 1 h. Detection was performed with 3.3-diaminobenzidine tetrachlorohydrochloride as a chromogen (Dako, Denmark), and sections were counterstained with haematoxylin.

Images were acquired with the iScan Coreo Au scanner (Ventana Medical Systems, Roche Diagnostics, Madrid, Spain) and visualised with Image Viewer software version 3.1 (Ventana Medical Systems). Images were captured at 5 × , 10 × , and 40 × magnification.

Statistical analysis

All analyses were performed using IBM® SPSS® Statistics version 26.0.0.0 (IBM Corp., Endicott, NY, USA) and represented using Origin Pro version 8.5 for Windows. The normality of the data was evaluated using the Shapiro-Wilk test. Descriptive data are presented as the mean and standard deviation when the data followed a normal distribution. Some results from the coating physicochemical characterisation, such as thickness, contact angle, and roughness, were statistically analysed. Statistical comparisons were performed using variance analysis (ANOVA) with a significance level of $p = 0.05$, followed by the Tukey test to identify differences between groups. For non-normally distributed data, descriptive statistics are presented as the median and interquartile range. A non-parametric Kruskal–Wallis test was used to compare more than three groups, and a Wilcoxon test was used to compare two groups. All tests were performed at least in triplicate.

Data availability

The data that support the findings of this study are available from the corresponding author upon reasonable request. The graphical abstract has been created in BioRender: Aguilera correa, J. (2025) https://BioRender.com/ak7ff0n.

Received: 13 November 2024; Accepted: 25 March 2025;
Published online: 10 April 2025

References

1. Xu, Y. et al. Microbiological diagnosis of device-related biofilm infections. *APMIS* **125**, 289–303 (2017).
2. Benito, N. et al. The different microbial etiology of prosthetic joint infections according to route of acquisition and time after prosthesis implantation, including the role of multidrug-resistant organisms. *J. Clin. Med* **8**, 673 (2019).
3. Zardi, E. M. & Franceschi, F. Prosthetic joint infection. A relevant public health issue. *J. Infect. Public Health* **13**, 1888–1891 (2020).
4. Ratner, B. D., Hoffman, A. S., Schoen, F. J. & Lemons, J. E. *Introduction to Biomaterials Science: An Evolving, Multidisciplinary Endeavor," in Biomaterials Science: An Introduction to Materials in Medicine*. https://doi.org/10.1016/C2009-0-02433-7 (Elsevier, 2020).
5. Drain, N. P. et al. High mortality after total knee arthroplasty periprosthetic joint infection is related to preoperative morbidity and the disease process but not treatment. *J. Arthroplast*. **37**, 1383–1389 (2022).
6. DeKeyser, G. J. et al. Socioeconomic status may not be a risk factor for periprosthetic joint infection. *J. Arthroplast*. **35**, 1900–1905 (2020).
7. Benito, N. et al. Time trends in the aetiology of prosthetic joint infections: a multicentre cohort study. *Clin. Microbiol. Infect*. **22**, 732.e1–732.e8 (2016).
8. Freiberg, J. A. et al. Restriction of arginine induces antibiotic tolerance in *Staphylococcus aureus*. *Nat. Commun*. **15**, 6734 (2024).
9. Kanellakopoulou, K. & Giamarellos-Bourboulis, E. J. Carrier systems for the local delivery of antibiotics in bone infections. *Drugs* **59**, 1223–1232 (2000).
10. Toirac, B. et al. Influence of addition of antibiotics on chemical and surface properties of sol-gel coatings. *Materials* **15**, 4752 (2022).
11. Esteban, J., Vallet-Regí, M. & Aguilera-Correa, J. J. Antibiotics- and heavy metals-based titanium alloy surface modifications for local prosthetic joint infections. *Antibiotics (Basel)* https://doi.org/10.3390/antibiotics10101270 (2021).
12. Gallo, J. et al. Silver nanocoating technology in the prevention of prosthetic joint infection. *Materials* **9**, 337 (2016).
13. Garcia-Casas, A., Aguilera-Correa, J. J., Mediero, A., Esteban, J. & Jimenez-Morales, A. Functionalization of sol-gel coatings with organophosphorus compounds for prosthetic devices. *Colloids Surf. B Biointerfaces* **181**, 973–980 (2019).
14. Toirac, B., Aguilera-Correa, J. J., Mediero, A., Esteban, J. & Jiménez-Morales, A. The antimicrobial activity of micron-thin sol–gel films loaded with linezolid and cefoxitin for local prevention of orthopedic prosthesis-related infections. *Gels* **9**, 176 (2023).
15. El hadad, A. A. et al. Preparation of sol–gel hybrid materials from γ-methacryloxypropyltrimethoxysilane and tetramethyl orthosilicate: study of the hydrolysis and condensation reactions. *Colloid Polym. Sci*. **289**, 1875–1883 (2011).
16. Toirac, B. et al. Electrochemical characterization of coatings for local prevention of Candida infections on titanium-based biomaterials. *Prog. Org. Coat*. **146**, 105681 (2020).
17. Mediero, A. et al. Ticagrelor regulates osteoblast and osteoclast function and promotes bone formation in vivo *via* an adenosine-dependent mechanism. *FASEB J*. **30**, 3887–3900 (2016).
18. Mediero, A., Wilder, T., Perez-Aso, M. & Cronstein, B. N. Direct or indirect stimulation of adenosine A $_{2A}$ receptors enhances bone regeneration as well as bone morphogenetic protein-2. *FASEB J*. **29**, 1577–1590 (2015).
19. Jacobson, K. A. & Gao, Z.-G. Adenosine receptors as therapeutic targets. *Nat. Rev. Drug Discov*. **5**, 247–264 (2006).
20. Mediero, A., Perez-Aso, M. & Cronstein, B. N. Activation of adenosine A2A receptor reduces osteoclast formation via PKA- and ERK1/2-mediated suppression of NFκB nuclear translocation. *Br. J. Pharm*. **169**, 1372 (2013).
21. Mediero, A. et al. Adenosine A $_{2A}$ receptor activation prevents wear particle–induced osteolysis. *Sci. Transl. Med*. https://doi.org/10.1126/scitranslmed.3003393 (2012).
22. Ishack, S., Mediero, A., Wilder, T., Ricci, J. L. & Cronstein, B. N. Bone regeneration in critical bone defects using three-dimensionally printed β-tricalcium phosphate/hydroxyapatite scaffolds is enhanced by coating scaffolds with either dipyridamole or BMP-2. *J. Biomed. Mater. Res B Appl. Biomater*. **105**, 366–375 (2017).
23. Conesa-Buendía, F. M. et al. Tenofovir causes bone loss via decreased bone formation and increased bone resorption, which can be counteracted by dipyridamole in mice. *J. Bone Miner. Res*. **34**, 923–938 (2019).
24. Arenas, M. A. et al. Doped TiO2 anodic layers of enhanced antibacterial properties. *Colloids Surf. B Biointerfaces* **105**, 106–112 (2013).
25. Garlito-Díaz, H. et al. A new antifungal-loaded sol-gel can prevent *Candida albicans* prosthetic joint infection. *Antibiotics* **10**, 711 (2021).
26. Aguilera-Correa, J. J. et al. A new antibiotic-loaded sol-gel can prevent bacterial prosthetic joint infection: from in vitro studies to an in vivo model. *Front. Microbiol*. https://doi.org/10.3389/fmicb.2019.02935 (2020).

27. Alibakhshi, E., Akbarian, M., Ramezanzadeh, M., Ramezanzadeh, B. & Mahdavian, M. Evaluation of the corrosion protection performance of mild steel coated with hybrid sol-gel silane coating in 3.5 wt.% NaCl solution. *Prog. Org. Coat*. **123**, 190–200 (2018).
28. El hadad, A. A. et al. Triethylphosphite as a network forming agent enhances in vitro biocompatibility and corrosion protection of hybrid organic–inorganic sol–gel coatings for Ti6Al4V alloys. *J. Mater. Chem. B* **2**, 7955–7963 (2014).
29. El hadad, A. A. et al. Enhancing in vitro biocompatibility and corrosion protection of organic–inorganic hybrid sol–gel films with nanocrystalline hydroxyapatite. *J. Mater. Chem. B* **2**, 3886–3896 (2014).
30. Vogelsberger, W., Seidel, A. & Fuchs, R. Contribution to the determination of kinetic parameters of the sol–gel transformation by rheological measurements. *J. Colloid Interface Sci*. **230**, 268–271 (2000).
31. Hernández-Escolano, M., Ramis, X., Jiménez-Morales, A., Juan-Díaz, M. & Suay, J. Study of the thermal degradation of bioactive sol–gel coatings for the optimization of its curing process. *J. Therm. Anal. Calorim*. **107**, 499–508 (2012).
32. W. C. ASTM International, ASTM D3359-02, Standard Test Methods for Measuring Adhesion by Tape Test, *ASTM Standards*. https://doi.org/10.1520/D3359-02 (2009).
33. Romero-Gavilán, F. et al. Control of the degradation of silica sol-gel hybrid coatings for metal implants prepared by the triple combination of alkoxysilanes. *J. Non Cryst. Solids* **453**, 66–73 (2016).
34. Juan-Díaz, M. J. et al. Study of the degradation of hybrid sol–gel coatings in aqueous medium. *Prog. Org. Coat*. **77**, 1799–1806 (2014).
35. Carbonell, D. J. et al. Scanning electrochemical microscopy characterization of sol-gel coatings applied on AA2024-T3 substrate for corrosion protection. *Corros. Sci*. **111**, 625–636 (2016).
36. Faghihi, S., Li, D. & Szpunar, J. A. Tribocorrosion behaviour of nanostructured titanium substrates processed by high-pressure torsion. *Nanotechnology* **21**, 485703 (2010).
37. Jianguo, L., Gaoping, G. & Chuanwei, Y. EIS study of corrosion behaviour of organic coating/Dacromet composite systems. *Electrochim. Acta* **50**, 3320–3332 (2005).
38. Tiringer, U., Durán, A., Castro, Y. & Milošev, I. Self-healing effect of hybrid sol-gel coatings based on GPTMS, TEOS, SiO_2 nanoparticles and $Ce(NO_3)_3$ applied on aluminum alloy 7075-T6. *J. Electrochem Soc*. **165**, C213–C225 (2018).
39. Tam K. & Torres, V. J. *Staphylococcus aureus* secreted toxins and extracellular enzymes. *Microbiol. Spectr*. https://doi.org/10.1128/microbiolspec.GPP3-0039-2018 (2019).
40. Aguilera-Correa, J. J. et al. Antibiotic delivery from bone-targeted mesoporous silica nanoparticles for the treatment of osteomyelitis caused by methicillin-resistant *Staphylococcus aureus*. *Acta Biomater*. **154**, 608–625 (2022).
41. Giacometti, A. Prophylactic efficacy of linezolid alone or combined with levofloxacin and vancomycin in a rat subcutaneous pouch model of graft infection caused by *Staphylococcus epidermidis* with intermediate resistance to glycopeptides. *J. Antimicrob. Chemother*. **52**, 724–726 (2003).
42. Becker, K., Heilmann, C. & Peters, G. Coagulase-negative Staphylococci. *Clin. Microbiol. Rev*. **27**, 870–926 (2014).
43. Rupp, M. E. & Archer, G. L. Coagulase-negative staphylococci: pathogens associated with medical progress. *Clin. Infect. Dis*. **19**, 231–245 (1994).
44. Lewis, R. E., Chamilos, G., Prince, R. A. & Kontoyiannis, D. P. Pretreatment with empty liposomes attenuates the immunopathology of invasive pulmonary aspergillosis in corticosteroid-immunosuppressed mice. *Antimicrob. Agents Chemother*. **51**, 1078–1081 (2007).
45. Neuhauser, M. M. et al. Antibiotic resistance among gram-negative bacilli in US intensive care units. *J. Am. Med. Assoc*. **289**, 885 (2003).
46. Odenholt, I., Löwdin, E. & Cars, O. Bactericidal effects of levofloxacin in comparison with those of ciprofloxacin and sparfloxacin. *Clin. Microbiol. Infect*. **4**, 264–270 (1998) .
47. Kohanski, M. A., Dwyer, D. J. & Collins, J. J. How antibiotics kill bacteria: from targets to networks. *Nat. Rev. Microbiol* **8**, 423–435 (2010).
48. Almeida-Santos, A. C. et al. The healthy human gut can take it all: vancomycin-variable, linezolid-resistant strains and specific bacteriocin-species interplay in *Enterococcus* spp. *Appl. Environ. Microbiol*. https://doi.org/10.1128/aem.01699-24 (2025).
49. Campos, J. D. S., Hoppe, L. Y., Duque, T. L. A., de Castro, S. L. & Oliveira, G. M. Use of noninvasive parameters to evaluate swiss webster mice during *Trypanosoma cruzi* experimental acute infection. *J. Parasitol*. **102**, 280–285 (2016).
50. Gawade, A., Kuchekar, A., Boldhane, S. & Baheti, A. Improvement of physicochemical and solubility of dipyridamole by cocrystallization technology. *J. Drug Deliv. Therap*. **11**, 43–48 (2021).
51. Xi, Z., Sharma, N., Paprikar, A. & Lin, S. Development and evaluation of dipyridamole sustained release tablets containing micro-environmental pH modifiers. *J. Drug Deliv. Sci. Technol*. **54**, 101231 (2019).
52. Anilkumar, A., Krishna Murthy, T. E. G. & Rani, A. P. Development of pH independent drug release system for dipyridamole. *Indian J. Pharm. Educ. Res*. **52**, 374–380 (2018).
53. "Product Information—Dipyridamole", CaymanChem webpage.
54. El Helou, O. C. et al. Outcome of enterococcal prosthetic joint infection: is combination systemic therapy superior to monotherapy? *Clin. Infect. Dis*. **47**, 903–909 (2008).
55. Schmid, A. et al. Monotherapy versus combination therapy for multidrug-resistant Gram-negative infections: systematic review and meta-analysis. *Sci. Rep*. **9**, 15290 (2019).
56. Greimel, F. et al. Efficacy of antibiotic treatment of implant-associated *Staphylococcus aureus* infections with moxifloxacin, flucloxacillin, rifampin, and combination therapy: an animal study. *Drug Des. Dev. Ther*. **11**, 1729–1736 (2017).
57. Bouza, E. & Muñoz, P. Monotherapy versus combination therapy for bacterial infections. *Med. Clin. North Am*. **84**, 1357–1389 (2000).
58. Samuel, J. R. & Gould, F. K. Prosthetic joint infections: single versus combination therapy. *J. Antimicrob. Chemother*. **65**, 18–23 (2010).
59. Rigo-Bonnin, R. et al. Development and validation of a measurement procedure based on ultra-high performance liquid chromatography-tandem mass spectrometry for simultaneous measurement of β-lactam antibiotic concentration in human plasma. *Clin. Chim. Acta* **468**, 215–224 (2017).
60. Nagarajan, S., Sankar, V., Bejoymohandas, K. S., Duan, Y. & Zhang, J. Influence of branched polyester chains on the emission behavior of dipyridamole molecule and its biosensing ability. *ACS Omega* **3**, 15530–15537 (2018).
61. White, R. L., Burgess, D. S., Manduru, M. & Bosso, J. A. Comparison of three different in vitro methods of detecting synergy: time-kill, checkerboard, and E test. *Antimicrob. Agents Chemother*. **40**, 1914–1918 (1996).
62. Odds, F. C. Synergy, antagonism, and what the chequerboard puts between them. *J. Antimicrob. Chemother*. **52**, 1–1 (2003).
63. Esteban, J. et al. Evaluation of quantitative analysis of cultures from sonicated retrieved orthopedic implants in diagnosis of orthopedic infection. *J. Clin. Microbiol*. **46**, 488–492 (2008).
64. Herigstad, B., Hamilton, M. & Heersink, J. How to optimize the drop plate method for enumerating bacteria. *J. Microbiol. Methods* **44**, 121–129 (2001).

Acknowledgements

This publication is part of the R + D + i Project PID2023-148002OB-I00, funded by MICIU/AEI/10.13039/501100011033 and by FEDER/EU. The authors would like to thank Dr Raul Rigo-Bonnin (Department of Clinical Laboratory, Hospital Universitario de Bellvitge, IDIBELL, Barcelona, Spain) for his technical support with the UHPLC/MS-MS method. This research was supported by CIBER—Consorcio Centro de Investigación Biomédica en Red-(CB 2021), Instituto de Salud Carlos III, Ministerio de Ciencia e Innovación and Unión Europea—NextGenerationEU. A.M. was supported by grants from Instituto de Salud Carlos III through the Miguel Servet program (CP15/00053, CPII20/00017) co-funded by Union Europea.

Author contributions

The conception and design of the study were carried out by A.J.-M., J.E., A.M., J.J.A.-C., and F.M. The acquisition and analysis of the data were performed by B.T. and the interpretation was done by A. S.-G., B.T., A.J.-M., B.T., F.M., J.E., and J.J.A.-G. Surface characterisation (AFM) was performed by M.M. HPLC measurements were carried out by O.M. Microbiological assays were performed by B.T., J.J.A.-C., A.M., and B.C. The interpretation of the data was done by A.J.-M., B.T., F.M., J.E., J.J.A.-G. Drafting the article was done by A.J.-M., A.S.-G., and B.T. Critical revision and final approval of the version to be submitted was carried out by all authors.

Competing interests

J.E. received travel grants from Pfizer and conference fees from bioMérieux and Heraeus. The funders had no role in the design of the study, the collection, analyses, or interpretation of data; the writing of the manuscript, or in the decision to publish the results. The remaining authors declare no conflict of interest. The antibiotics-loaded sol–gel used in this study is one of the products protected by the patent entitled *Procedure for Obtaining a Sol–Gel Coating, Composition Coating and Use of the Same*; P201730628; Antonia Jiménez Morales, Amaya García Casas, Jaime Esteban Moreno, John Jairo Aguilera Correa; Spain. The use of dipyridamole as a novel osteostimulant therapy in this study is one of the products protected by the patent entitled *Tissue repair devices and scaffolds*; 20160262894; Brouce N. Cronstein, Aranzazu Mediero Muñoz, John Ricci, Stephen Ishack; United States.

Additional information

Supplementary information The online version contains supplementary material available at https://doi.org/10.1038/s43246-025-00790-7.

Correspondence and requests for materials should be addressed to Ángela Solís-Garrido or John Jairo Aguilera-Correa.

Peer review information *Communications Materials* thanks Lia Rimondini and the other, anonymous, reviewer(s) for their contribution to the peer review of this work. Primary Handling Editors: Steven Caliari and Jet-Sing Lee. [A peer review file is available.]